AD_____

Award Number: W81XWH-04-1-0023

TITLE: MR Imaging Based Treatment Planning for Radiotherapy of Prostate Cancer

PRINCIPAL INVESTIGATOR: Lili Chen, Ph.D.

CONTRACTING ORGANIZATION: Fox Chase Cancer Center
                          Philadelphia, PA 19111

REPORT DATE: February 2006

TYPE OF REPORT: Annual

PREPARED FOR: U.S. Army Medical Research and Materiel Command
               Fort Detrick, Maryland 21702-5012

REPORT DOCUMENTATION PAGE

Form Approved
OMB No. 0704-0188

Public reporting burden for this collection of information is estimated to average 1 hour per response, including the time for reviewing instructions, searching existing data sources, gathering and maintaining the data needed, and completing and reviewing this collection of information. Send comments regarding this burden estimate or any other aspect of this collection of information, including suggestions for reducing this burden to Department of Defense, Washington Headquarters Services, Directorate for Information Operations and Reports (0704-0188), 1215 Jefferson Davis Highway, Suite 1204, Arlington, VA 22202-4302. Respondents should be aware that notwithstanding any other provision of law, no person shall be subject to any penalty for failing to comply with a collection of information if it does not display a currently valid OMB control number. **PLEASE DO NOT RETURN YOUR FORM TO THE ABOVE ADDRESS.**

1. REPORT DATE *(DD-MM-YYYY)*	2. REPORT TYPE	3. DATES COVERED *(From - To)*
01-02-2006	Annual	1 Feb 2005 – 31 Jan 2006

4. TITLE AND SUBTITLE
MR Imaging Based Treatment Planning for Radiotherapy of Prostate Cancer

5a. CONTRACT NUMBER

5b. GRANT NUMBER
W81XWH-04-1-0023

5c. PROGRAM ELEMENT NUMBER

6. AUTHOR(S)
Lili Chen, Ph.D.

E-mail: Lili.Chen@fccc.edu

5d. PROJECT NUMBER

5e. TASK NUMBER

5f. WORK UNIT NUMBER

7. PERFORMING ORGANIZATION NAME(S) AND ADDRESS(ES)

Fox Chase Cancer Center
Philadelphia, PA 19111

8. PERFORMING ORGANIZATION REPORT NUMBER

9. SPONSORING / MONITORING AGENCY NAME(S) AND ADDRESS(ES)
U.S. Army Medical Research and Materiel Command
Fort Detrick, Maryland 21702-5012

10. SPONSOR/MONITOR'S ACRONYM(S)

11. SPONSOR/MONITOR'S REPORT NUMBER(S)

12. DISTRIBUTION / AVAILABILITY STATEMENT
Approved for Public Release; Distribution Unlimited

13. SUPPLEMENTARY NOTES

14. ABSTRACT
This work is aimed at MRI-based treatment planning for radiation therapy. The tasks for the second year include (a) Evaluate MRI-based prostate treatment planning dose calculation; (b) Develop practical methods for heterogeneity correction for MR-based dose calculation and (c) Implement and validate a MRI-based Monte Carlo dose verification system for IMRT QA. We have quantified the residual distortions and developed computer software to reduce them using point-by point corrections for large patients (lateral dimension up to 42 cm). We have verified dosimetric accuracy and consistency for MR based IMRT treatment planning for prostate cancer using the Monte Carlo method. Our results showed that for IMRT treatments with coplanar beam arrangements, the mean dose values of the CTV for homogeneous geometry based on CT were about 2% higher than those for heterogeneous geometry based on CT. The difference in the mean CTV dose between homogenous MRI and heterogeneous CT geometries was about 3% and less. We have also studied heterogeneity corrections for patients with hip replacements (prostheses).

15. SUBJECT TERMS
MR-based treatment planning, Dosimetry, Radiotherapy, Monte Carlo dose verification

16. SECURITY CLASSIFICATION OF:			17. LIMITATION OF ABSTRACT	18. NUMBER OF PAGES	19a. NAME OF RESPONSIBLE PERSON USAMRMC
a. REPORT U	**b. ABSTRACT** U	**c. THIS PAGE** U	UU	64	**19b. TELEPHONE NUMBER** *(include area code)*

Standard Form 298 (Rev. 8-98)
Prescribed by ANSI Std. Z39.18

Table of Contents

Introduction

This project is aimed at exploring MR imaging based treatment planning for radiotherapy of prostate cancer. We have proposed to work on the second task for the second research year. The tasks include (1) evaluating MRI-based prostate treatment planning dose calculation; (2) to develop practical methods for heterogeneity correction for MRI-based dose calculation and (3) to implement and validate a MRI-based Monte Carlo dose verification system for IMRT QA. In the following we describe our work for the second year.

Body

In this annual report we report on the research accomplishments associated with the tasks outlined in the approved "Statement of Work" task 2 between Mar. 1, 2005 and Feb. 28, 2006. We will provide detailed information below for the results in the second year.

Task 2. Investigate MRI-based treatment planning dose calculation

Evaluate MRI-based prostate treatment planning dose calculation

During this period, we have focused on MR image distortion correction to further improve the accuracy of dose calculation for MR based treatment planning for prostate cancer. A paper entitled "investigation of MR image distortion for radiotherapy treatment planning of prostate cancer" has been accepted by Physics in Medicine and Biology for publication (Chen et al 2006a). We also used the Monte Carlo method to verify dosimetric accuracy and consistency for MR based IMRT treatment planning for prostate cancer. A paper entitled "Monte Carlo dose verification of MR image based IMRT treatment planning for prostate cancer" has been submitted to Physics in Medicine and Biology (Chen et al 2006b). The two manuscripts are also attached to this report. We summarize the results and conclusions of these studies as follows.

(1) We have focused on MR image distortion correction to further improve the accuracy of dose calculation for MR based treatment planning for prostate cancer. Our studies showed that, with our routine clinical 3-dimensinal fast spin echo sequences (3DFSE, 256 x 256, 1.855 mm pixel, TR = 140 ms, TE = 3000 ms, BW readout gradient > 100 Hz/pixel), there was no patient-induced distortions. Therefore, the residual machine specific geometrical distortions after the gradient distortion correction (GDC) could be quantified by phantom measurements and further reduced by our point-by-point correction technique. The effective field of views (FOV_{eff}) of the scanner were established based on the actual viewable areas with adequate geometric distortion corrections (ensuring < 5 mm distortion error). The effective FOV_{eff} for prostate imaging using a standard FOV of 48 cm has been expanded from 36 cm using the existing GDC software to 42 cm using the point-by-point distortion correction technique developed in this work. Our results indicated that, with the distortion maps established in this work, we could correct MR geometrical distortions for patients of lateral dimensions up to 42 cm. Significant improvement in dose calculation has been achieved based on a 1-2 cm improvement in patient external contour determination.

(2) We have performed the Monte Carlo method to verify dosimetric accuracy and consistency for MR based IMRT treatment planning for prostate cancer. The Monte Carlo code used in this work was MCSIM, which is an EGS4/PRESTA user code developed at Fox Chase Cancer Center (FCCC) (Ma et al 2002). The beam information was represented using a source model,

4

which was built based on measured beam data (Jiang et al 2000, 20001; Yang et al 2004), and validated for Monte Carlo dose calculation for photon beams from our Siemens accelerators. During the calculation, the multi-leaf collimator leakage effect was taken into account when intensity maps were reconstructed from a plan. The accuracy of the dose calculation was better than 2% compared with measured data (Li et al 2000). For each patient, an RTP file from the Corvus treatment planning system that includes patient setup parameters and beam and leaf-sequence information was used for the Monte Carlo dose calculation. For the Monte Carlo simulation, the electron and photon energy cutoffs, ECUT and PCUT, for particle transport were set to 700 keV and 10 keV, respectively. The energy thresholds for δ ray production (AE) and for Bremsstrahlung production (AP) were also set to 700 keV and 10 keV, respectively. The maximum fractional energy loss per electron step (ESTEP) was set to 0.04 and the default parameters were used for the PRESTA algorithm. The patient geometry used for the Monte Carlo calculations was created based on both CT and MR data. The materials and mass densities of CT based geometries were converted from the CT numbers based on a piecewise linear conversion curve that was given by Ma et al (1999). Seventy million particle histories were used in the Monte Carlo simulations to achieve less than 0.5% statistical uncertainties to the target dose for all the IMRT plans. Each photon was split 20 times to improve the simulation efficiency using the photon-splitting technique implemented in MCSIM.

(3) We have performed CT-based IMRT Monte Carlo dose calculations with and without heterogeneity corrections in order to investigate the heterogeneity effect caused by different beam angle arrangements. Based on the results, MR-based IMRT dose calculations were performed using either uniform density geometry or uniform density geometry with bulk electron density assigned to bony structures. For the plans with insignificant inhomogeneity effect, uniform geometries with water density were used in the MR-based dose calculation. For the plans that bony structure constitutes a large part of volume irradiated, uniform density geometry with bulk electron density assigned to bony structures was used in the MR-based dose calculation. Each IMRT plan was evaluated based on isodose distributions and dose volume histograms (DVHs) with CT-based or MR-based dose calculations. The clinical target volume (CTV) was chosen for the dose-volume comparison. Clinical quantities such as the mean dose, maximum and minimum dose received by the CTV and the critical structures were compared. The maximum dose was defined as the highest dose received by 1% of the target volume and the minimum dose was defined as the lowest dose received by 99% of the target volume, respectively. Other parameters such as the dose at the isocenter and the dose received by 95% and 5% of the CTV were also compared. The paired CT and MR data for any patients in this work were pre-processed to have the same pixel resolution. The internal contours of the targets and critical organs were contoured by oncologists on the fused CT-MR images. A special computer code was developed to convert the patient CT and MR image data from the DICOM format to geometries specially formatted for the MCSIM code.

Develop practical methods for heterogeneity correction for MRI-based dose calculation

Our preliminary results demonstrated that MR-based planning was equally good as CT-based planning for prostate cancer with homogeneity geometry in the dose calculation. The differences between CT and MR-based dose calculations came from the setup uncertainties in the CT and MR image acquisition (Chen et al 2005). For prostate cancer, the following beam arrangements were commonly used for routine treatment IMRT plans at Fox Chase Cancer Center: 1) one anterior, 2) two or four anterior oblique, 3) two lateral and 4) two or four posterior oblique beams. The couch angles were set

as zero (i.e. coplanar beam arrangements). Our results showed insignificant differences in the clinical quantities between MR-based dose calculations with uniform water equivalent geometry and CT-based dose calculations with heterogeneity correction. The maximum differences were less than 4% and the averaged differences over the 10 IMRT plans were less then 1.6% for all the quantities in the comparison, indicating that the uniform geometry was a good approach with our commonly used beam arrangements. These results were consistent with previous findings (Chen at al 2004 and Yang et al 2004).

However, for some clinical cases non-coplanar beam arrangements were needed to achieve better target dose coverage and rectal sparing. Our results showed that with non-coplanar beam arrangements more than 10% differences between plans with and without heterogeneity correction were found in the single beam calculations for the beam going through a large amount of pelvic bones. To utilize MR-based planning for the treatment with large amount of pelvic bones irradiated, heterogeneity corrections must be taking into account and a bulk-density can be assigned to bony structures as proposed by this project since there is no point-to-point correlation between MR signal intensities and electron densities of the materials imaged (Lee and Bollet 2003, Chen et al 2004b). Various bulk-densities (between 1.5 and 2.2 g/cm^3) were assigned to the femurs and femoral heads in this work. Our results showed that $1.8 g/cm^3$ is the optimal value for the bulk-density assignment.

For those beams with gantry/table angles as 275/340, 85/20 and 85/0, the differences in the average target doses were decreased from about 10% with uniform water equivalent geometry to about 3% or less after assigning $1.8 g/cm^3$ bulk density to femurs and femoral heads. The changes in DVHs using CT data with $1.8 g/cm^3$ bulk density for the femurs and femoral heads also confirmed our findings.

We also have been studying heterogeneity corrections for patients with hip replacement (prostheses) with MR-based treatment planning.

Implement and validate a MRI-based Monte Carlo dose verification system for IMRT QA

At FCCC, we have implemented Monte Carlo simulations as a quality assurance (QA) tool for IMRT dose verification using the EGS4/MCSIM Monte Carlo program (Ma et al 1999, 2000, 2002), In which a patient's CT and MLC leaf sequences are directly used to reconstruct the dose to be received by the patient. We have been working on MRI-based IMRT QA phantoms and perform dose calculations to determine monitor units (MU) for IMRT plans and then compare with ion chamber measurements. We will integrate MRI in this Monte Carlo QA process for IMRT MU calculation and beam delivery verification.

Key Research Accomplishments

We have accomplished the following tasks:

- We have developed a point-by point distortion correction technique to correct MR geometrical residual distortions with the use of the gradient distortion correction (GDC) software.

- We have developed practical methods for heterogeneity correction for MRI-based dose calculation in inhomogeneous patient anatomy.

- We have used the Monte Carlo method to validate the dose accuracy and consistency for MR-based treatment planning of prostate cancer.

Reportable Outcomes

Peer-reviewed papers resulting from or supported in part by this grant:

- Chen Z, Ma C-M, Paskalev K, Li J, Yang J, Richardson T, Palacio L, Xu X and **Chen L**. Investigation of MR Image Distortion for Radiotherapy Treatment Planning of Prostate Cancer. cancer *Phys. Med. Biol.* In Press (2006a) in press

- Chen Z, Ma C-M, Yang J, Li J, Luo W, Fan J, Paskalev K.A, Price Jr R A, Chen Y and **Chen L,** Monte Carlo dose verification of MR image based IMRT treatment planning for prostate cancer. *Phys. Med. Biol.* submitted (2006b)

- Luo W, Li J, Price R, **Chen L,** Yang J, Fan J, Chen Z, McNeeley S and Ma CM. Monte Carlo based IMRT dose verification using MLC log files and R/V outputs *Medical Physics.* Conditionally accepeted (2006)

- Yang J, Li J, **Chen L**, Price R, McNeeley S, Qin L,Wang L, Xiong W, Ma C-M. Dosimetric verification of IMRT treatment planning using Monte Carlo simulations for prostate cancer. *Phys Med Biol.* 50(5): 869-78 (2005)

- Yuh EL, Shulman SG, Mehta SA, Xie J, **Chen L,** Frenkel V, Bednarski MD and Li KCP. Delivery of a Systemic Chemotherapeutic Agent to Tumors Using Focused Ultrasound: study in a murine model *Radiology* February 1, 2005; 234(2): 431 - 437.

- Wang L, Li J, Paskalev K, Hoban P, Luo W, **Chen L**, McNeeley S, Price R, Ma C-M. Commissioning and quality assurance of a commercial stereotactic treatment planning system for extracrenial IMRT, *Journal of Clinic Appl. Med. Phys*. 2006 in press

- Wang, L, Hoban, P, Paskalev, K, Yang, J, Li, J. S, **Chen, L,** Xiong, W, Ma, C.M. Dosimetric Advantage and Clinical Implication of a micro-Multileaf Collimator in the Treatment of Prostate with Intensity Modulated Radiotherapy. *Medical Dosimetry*. 30 97-103 2005

Meeting abstracts resulting from or supported in part by this grant:

- **Chen L**, Zhu J, Xu x, Wand L, Paskalev K, Chen Z, Movsas B, Ma C. Image guided radiation therapy: investigation of interfraction setup and external contour variation for prostate IMRT using CT and MRI. Proc. *Medical Physics*, 32(6), 1928, 2005.

- Fan J, Li J, **Chen L**, Xiong W, Stathakis S, Luo W Plessis F Du Ma C. A practical Monte Carlo MU veirification tool for IMRT quality assurance Proc. *Medical Physics*, 32(6), 1979, 2005.

- Ma C, Li J, Price R, **Chen L**, Konski A, Watlins-Bruner D, Pollack A. Treatment optimization for prostate IMRT incorporating utility analysis and patient decisions. Proc. *Medical Physics*, 32(6), 2039, 2005.

- Chen Z, Yang J, Li J, Paskalev K, Ma C, **Chen L**. Monte Carlo dose verification for MRI-based treatment planning of prostate cancer. Proc. *Medical Physics*, 32(6), 1884, 2005.

- Yang J, Li J, **Chen L**, Chen Z, Luo W, Fan J, Stathakis S, Price R, Ma C. Mote Carlo investigation of heterogeneity effect for head and neck IMRT. Proc. *Medical Physics*, 32(6), 1886, 2005.

- L Chen, K Paskalev, J Zhu, X Xu, L Wang, R Price, E Horwitz, S Feigenberg, A Pollack, C Ma. Image Guided Radiation Therapy for Prostate IMRT: Rectum Volume Changes and Dosimetric Considerations. Proc. *International Journal of Radiation Oncology Biology Physics* 2005

Funding applied for based on work resulting from or supported in part by this grant:

Conclusions

We have made significant progress during our second-year investigation. We have successfully performed the tasks scheduled in the "Statement of Work". We have performed Mote Carlo dose calculations using MRI-derived homogenous geometry with heterogeneity corrections. We have developed a practical method of dose calculation for MR-based treatment planning in heterogeneous patient anatomy. We have developed a point-by-point distortion correction technique to correct the residual MRI distortions after the GDC. We have been working on the implementation and validation of a MRI-based Monte Carlo dose verification system for IMRT QA

References

Chen Z, Ma C-M, Paskalev K, Li J, Yang J, Richardson T, Palacio L, Xu X and **Chen L**. Investigation of MR Image Distortion for Radiotherapy Treatment Planning of Prostate Cancer. cancer *Phys. Med. Biol.* In Press (2006a) in press

Chen Z, Ma C-M, Yang J, Li J, Luo W, Fan J, Paskalev K.A, Price Jr R A, Chen Y and **Chen L** Monte Carlo dose verification of MR image based IMRT treatment planning for prostate cancer. *Phys. Med. Biol.* submitted (2006b)

Chen L, Zhu J, Xu X, Wang L, Paskalev K, Chen Z, Movsas B, and Ma C. Image Guided Radiation Therapy: Investigation of Interfraction Setup and External Contour Variation for Prostate IMRT Using CT and MRI *Phys. Med .*Vol. **32** 1928 (2005)

Chen L, Price R, Nguyen T-B, Wang L, J S Li, Qin L, Ding M, Palacio E, Ma C-M and Pollack A. Dosimetric evaluation of MRI-based treatment planning for prostate cancer *Phys. Med. Biol*. **49** 5157-5170 (2004)

Chen Z, Ma C-M et al Investigation of CT-MR Image Intensity Correlation for MRI-based Dose calculation. *Med. Phys*., Vol.**31** No. 6 (abstract) (2004b)

Jiang S B, Boyer A L, and Ma C-M 2001 Modeling the extrafocal radiation and monitor chamber backscatter for photon beam dose calculation *Med. Phys.* **28**, 55-66

Jiang S B, Deng J, Li J S, Pawlicki T, Boyer A L, and Ma C-M 2000 Modeling and commissioning of clinical photon beams for Monte Carlo treatment planning *XIII ICCR 2000* ed W Schlegel and T Bortfeld pp 434-6

Lee YK and Bollet M, 2003 Radiation Treatment Planning of Prostate Cancer Using Magnetic Resonance Imaging Alone, *Radiotherapy and Oncology* **66**:203-216

Li J S, Pawlicki T, Deng J, Jiang S B and Ma C-M 2000 Validation of a Monte Carlo dose calculation tool for radiotherapy treatment planning *Phys. Med. Biol*. **45** 2969-85

Ma C-M, Mok E, Kapur A, Findley D, Brain S, Forster K and Boyer A L. Clinical implementation of a Monte Carlo treatment planning system, Med. Phys. 26:2133-43 (1999)

Ma C M. Pawlicki T. Jiang S B, Mok E, Kapur a., L. Xing, L. Ma and A.L. Boyer, Monte Carlo verification of IMRT dose distributions from a commercial treatment planning optimization system, Phys. Med. Biol., 45:2483-95 (2000)

Ma C-M. Li J S, Pawlicki T, Jiang S.B, Deng J, A Monte Carlo dose calculation tool for radiotherapy treatment planning, Med. Phys. 47:1671-89 (2002)

Ma C-M, Li J S, Pawlicki T, Jiang S B, Deng J, Lee M C, Koumrian T, Luxton M and Brain S 2002b A Monte Carlo dose calculation tool for radiotherapy treatment planning *Phys. Med. Biol.* **47** 1671-89

Ma C-M, Mok E, Kapur A, Pawlicki T, Findley D, Brain D S, Forster K, and A. L. Boyer A L 1999 Clinical implementation of a Monte Carlo treatment planning system *Med. Phys.* **26** 2133-43

Yang J, Li J S, Qin L, Xiong W and Ma C-M 2004 Modeling of electron contamination in clinical photon beams for Monte Carlo dose calculation *Phys. Med. Biol*. **49** 2657-73

Yang J, Li J S, Chen L, Price R, McNeeley S, Qin L, Wang L, W Xiong and Ma C-M 2005 Dosimetric verification of IMRT treatment planning using Monte Carlo simulations for prostate cancer *Phys. Med. Biol.* **50** 1-10.

Appendices

List of manuscripts quoted in the body of text:

Z. Chen, C.-M. Ma, K. Paskalev, J. Li, J. Yang, T. Richardson, L. Palacio, X. Xu and L. Chen. Investigation of MR Image Distortion for Radiotherapy Treatment Planning of Prostate Cancer *Phys. Med. Biol.* In press (2006a).

Z. Chen, C-M Ma, J. Yang, J. Li, W. Luo, J. Fan, K. A. Paskalev R. A. Price Jr, Y. Chen and L. Chen, Monte Carlo dose verification of MR image based IMRT treatment planning for prostate cancer *Phys. Med. Biol.* Submitted (2006b)

Investigation of MR Image Distortion for Radiotherapy Treatment Planning of Prostate Cancer

Z. Chen, C.-M. Ma, K. Paskalev, J. Li, J. Yang, T. Richardson, L. Palacio, X. Xu and L. Chen

Department of Radiation Oncology, Fox Chase Cancer Center, Philadelphia, Pennsylvania, 19111

E-mail: jay.chen@fccc.edu

Abstract

MR imaging based treatment planning for radiotherapy of prostate cancer is limited due to MR imaging system related geometrical distortions, especially for patients with large body sizes. On our 0.23 T open scanner equipped with the gradient distortion correction (GDC) software, the residual image distortions after the GDC were < 5 mm within the central 36 cm x 36 cm area for a standard 48 cm field of view (FOV). In order to use MR imaging alone for treatment planning the effect of residual MR distortions on external patient contour determination, especially for the peripheral regions outside the 36 cm x 36 cm area, must be investigated and corrected. In this work, we performed phantom measurements to quantify MR system related residual geometric distortions after the GDC and the effective FOV. Our results show that for patients with larger lateral dimensions (> 36 cm), the differences in patient external contours between distortion-free CT images and GDC-corrected MR images were 1-2 cm because of the combination of greater gradient distortion and loss of field homogeneity away from the isocenter and the uncertainties in patient setup during CT and MRI scans. The measured distortion maps were used to perform point-by-point corrections for patients with large dimensions inside the effective FOV. Using the point-by-point method, the geometrical distortion after the GDC were reduced to < 3mm for external contour determination and the effective FOV was expanded from 36 cm to 42 cm.

Keywords: MRI based treatment planning, Open MRI, Image distortion correction.

1. Introduction

Computed tomography (CT) has played a very important role in radiation treatment planning in modern radiotherapy. Based on the information provided by CT data, a treatment planning system can delineate patients' tumor volumes, external contours and critical anatomic structures, and obtain digitally constructed radiographs (DDR) for patient treatment setup and perform accurate dose calculations for treatment planning. Although CT based treatment planning has been considered as a "gold standard" in radiotherapy for years, it has long been recognized as having poor soft tissue contrast, which may bring uncertainties into treatment planning. For example, Khoo at al (1999) found that MRI provided improved definitions of both prostate and critical structures compared to CT. Additionally, Rasch at al (1999) found that the prostate volumes was 40% larger on CT than MR, in agreement with Roach et al (1996), who found that the prostate was 32% larger on CT than on MRI. Debois et al (1999) showed that improved rectal and prostate volumes delineation from MRI could lead to both improvement in target coverage and rectal sparing. As many investigators demonstrated (Zelefsky et al 1998, Pollack et al 1999, Pollack et al 2000, Hanks et al 1999, Hanks 1998), dose escalation with 3D conformal and recently IMRT increased local control while reducing complications in nearby critical structures. However, as dose levels are increased, the precise knowledge of tumor volumes and the accuracy of dose calculation and delivery become critical. Magnetic resonance (MR) imaging has been shown to provide more consistent tumor volume delineation in treatment planning due to its superior soft tissue contrast than CT for a variety of sites.

Although CT and MR fusion has been widely accepted as a practical approach for both accurate delineation (using MR data) and dose calculation (using CT data) it would be ideal that MRI could replace CT entirely for treatment planning, retaining the superior soft tissue contrast for image segmentation and at the same time eliminating the potential errors in image fusion due to (a) variations in patient setups between CT and MR and (b) uncertainties in target localization

between the two image modalities. Furthermore, MRI based treatment planning will avoid redundant CT imaging sessions, which in turn will avoid unnecessary radiation exposure to patients, reduce treatment costs, and save patient, staff and machine time. There has been a growing interest in the utilization of MRI based radiotherapy treatment planning for the past decade, and progress has been made in developing an effective MRI based method for treatment planning (Beavis et al 1998, Guo 1998, Mah et al 2002, Chen et al 2002, Michiels et al 1994, Chen et al 2003, Lee et at 2003).

It is well known that there are several technical challenges for MRI based treatment planning: (1) to minimize MR image geometrical distortions, (2) to incorporate sequences that reduce MR distortions, (3) to develop methods that can correct MR-related distortions, (4) to correlate MR signal intensity with the densities of the materials imaged and (5) to obtain MRI-derived DRR for patient setup.

We have been working extensively on developing MRI based treatment planning models for the last few years (Chen et al 2003, Chen et al 2004a, Chen et al 2004b, Chen et al 2004c). It has been generally accepted that there are no clinically significant differences in dose calculation between homogeneous and heterogeneous geometry for pelvis and it has been common practice to use homogenous geometry. We have implemented MRI-based prostate treatment planning at Fox Chase Cancer Center (FCCC). We have verified the dose calculation accuracy with unit-density geometry built for MR data. The agreement was within 2% with CT based dose calculation (Chen et al 2004a). An effective procedure has been achieved to derive MRI based DRRs for prostate cancer patient treatment setup (Chen et al 2004b).

Our clinical MR unit (0.23 T open MR system, Philips Medical Systems, Cleveland, OH) is equipped with the gradient distortion correction (GDC) software (Mah et al 2002). Comparisons of patients' MR and distortion-free CT images showed that the systematic geometrical distortions

were very small after the GDC for patients with 36 cm lateral dimensions and the dosimetric consequences due to these distortions were negligible for treatment planning. However, for patients with larger lateral dimensions, the differences in patient external contours between distortion-free CT images and GDC-corrected MR images were significant (1-2 cm) because of the combination of greater gradient distortion and loss of field homogeneity away from the isocenter and the uncertainties in patient setup during CT and MRI scans. The uncertainties on the external contours will lead to errors in beam path length determination, which in turn may result in dose errors of clinical significance. In order to implement MR-based treatment planning clinically, the effective FOV of our MR scanner must be investigated and expanded to include patients with larger lateral dimensions.

In this paper, we present the results of our MR image distortion investigation on a 0.23 T open scanner for prostate IMRT treatment planning. A point-by-point mapping technique is developed to further reduce residual gradient distortions after GDC post-processing. We will describe the technical aspects of our method and its implementation and validation. We will show that together with setup uncertainty quantification, the effective FOV of the scanner can be expanded to include almost all the prostate patients, and the uncertainties of patient external contours due to MR image distortions can be determined accurately.

2 Materials and Method

2.1. The MR scanner

The MR system used for this study was a 0.23 Tesla open scanner operating clinically in the department of Radiation Oncology at Fox Chase Cancer Center (figure 1). The MR scanner consists of two approximately 1 m diameter poles. The separation between the two poles is 47 cm. The MR scan table can be moved in orthogonal planes along a set of rails mounted on the floor and on an orthogonal set of rails built in the couch. A flat tabletop made of special material,

which is stiff and light, was inserted beneath the patient. A set of pads made of special foam was used to adjust the table height according to the patient size. The three triangulation lasers (center and laterals) identical to those used on the linear accelerators were used for patient positioning.

2.2. MR geometrical distortions and the GDC software

In MR imaging, each point in the imaging space is associated to a resonance frequency, which is generated by the linear magnetic field gradient. In one dimension, say the x direction, this can be expressed by:

$$\varpi(x) = \gamma(B_0 + xG_x) \tag{1}$$

where, B_0 and G_x are the main magnetic field intensity and the magnetic field gradient in the x direction respectively, and γ is the gyromagnetic ratio. It is common knowledge that non-uniformity of B_0 and non-linearity of G_x will introduce uncertainties to the images on the spatial localization of the different resonance frequencies because the way MR images are reconstructed. These uncertainties were defined as MR imaging geometrical distortions.

MR imaging geometrical distortions can be divided into machine-induced geometrical distortion and patient-induced geometrical distortion (Michiels et al 1994). The machine-induced MR geometrical distortion includes the main field in-homogeneity, gradient field non-linearity and eddy currents caused by the gradient switching. As it has been demonstrated by many investigators (Michiels et al 1994, Chang et al 1990, Sumanaweera et al 1994, Schad et al 1994), the distortions induced by gradient non-linearity and main magnetic field non-uniformity are stable and can be corrected independently of other machine induced distortions. The patient-induced geometrical distortions include susceptibility effects, chemical shift and flow, which generally cannot be corrected "once and for all" because of its patient dependency. However, due to the high receiver bandwidth (> 100 Hz/pixel) in the frequency encoding direction used in our routine scanning, and based on the fact that there is no patient-induced MR image artifacts

detected with 0.2 T low magnetic field using receiver bandwidth > 100 Hz/pixel in the frequency direction (Fransson et al 2001), the patient-induced geometrical distortion was considered negligible for our MR unit. Therefore, the machine-induced geometrical distortions to the images from our MR scanner can be detected, studied and corrected accurately.

A Federal Drug Administration (FDA) approved GDC software provided by the manufacturer was installed on our scanner for MR image post-processing. The effectiveness of the post-processing was evaluated using a standard phantom (F18 phantom) provided by the manufacturer (figure 1b). The F18 phantom is intended for evaluation of residual geometrical distortions in the images post-processed by the GDC software. The phantom consists of a rectangular grid of spherical markers in a single plane separated by 2.5 cm in both directions (17 columns and 15 rows). The phantom is 3 cm in thickness and supplied with a support structure that allows the F18 phantom to be fixed into a body/spine coil. The orientation of the marker plane can be selected to align with any of the fixed imaging planes. In our measurements, the F18 phantom was placed in the xy plane of the coordinate system (transverse plane) with $z = z_0$, x defined as horizontal and y as vertical.

It should be emphasized that MRI geometrical distortions are caused by non-uniformity of the magnetic field and gradient non-linearity in the 3-dimensional space. The residual distortions after the GDC are expected to be 3-dimensional. Since MRI does not provide electron density information required for inhomogeneity corrections in dose calculation and, for some sites like the prostate, these corrections are not clinically significant (Photon Treatment Planning Collaborative Working Group 1991), we have used homogeneous geometry for both CT-based and MRI-based treatment planning. The homogeneous geometry makes the distortion correction in the inferior-superior direction unnecessary in dose calculation. The only corrections needed in

MRI-based treatment planning are those in the transverse plane, which affect the patient external contours. In this study, only distortions in the transverse planes were considered.

The effective FOV after the GDC was established 36 cm within which the effect of residual MR distortions on patient external contours was less than 5 mm. A larger effective FOV is required for MRI-based treatment planning of patients with larger lateral dimensions. In this work we have quantified the residual distortions after the GDC in the areas outside the 36 cm FOV using the F18 phantom. A Synergy Body/Spine L coil was selected and the phantom (with the support structure) was inserted into the coil, guided by the laser beam. The coil was placed at the center of the 0.23T scanner with the phantom plane in the sagittal direction (the x and y plane of the coordinate system). The phantom was imaged at different positions with a small increment $\pm \Delta z$ in the z direction. The images were then exported in the DICOM format and transferred to our development environment for processing. Since each marker's geometrical position on the phantom is known (also can be calculated accurately knowing the position of the center of the phantom on the image), the distortions for the markers at different z positions can be quantified by comparison with the known geometrical positions of the markers. For each position along the z-direction, a mapping file, which records the distortions in the transverse plane, was derived based on the measurements of the markers, and a computer program was developed to correct the distortions point-by-point for any MR scans using the measured distortion maps stored in the files.

Since the F18 only has 17 markers in the horizontal direction and 15 in the vertical direction, the distortions outside the 40 x 35 cm^2 central area were measured by shifting the phantom left and right a few centimeters to determine the effective FOV.

2.3. The point-by-point distortion correction method

Based on the distorted images of the grid points at different z positions, correction maps can be derived by comparisons of the distorted images with the physical pattern of the grid on the F18 phantom. These maps can then be applied to rectify patient images acquired at the corresponding positions, using identical imaging sequences and parameter settings.

To quantify the distortion, i.e. the differences between the corresponding marker points of the F18 phantom and the image acquired from the scanner, a Cartesian coordinate is introduced, and the origin (0, 0) of the coordinate is set at the bottom left corner of the images. In the Cartesian coordinate, we define the distributions of the grid points as $\vec{r}_z^{\,p}(i,j)$ and $\vec{r}_z^{\,s}(i,j)$, where $\vec{r}_z^{\,p}(i,j)$ is the spatial distribution of the points on the F18 phantom and $\vec{r}_z^{\,s}(i,j)$ is the spatial distribution of the centers of the markers on the image scanned, respectively. The distortion maps can then be defined as:

$$\vec{M}_z(i,j) = \vec{r}_z^{\,p}(i,j) - \vec{r}_z^{\,s}(i,j) \qquad (2)$$

where $i = 1,2,...,17$ and $j = 1,2,...,15$.

Once the maps of the geometrical distortions of the markers are established, they can be used to correct the residual distortions of MR images.

Figure 2 demonstrates the principles of mapping the pixels within the area defined by 4 marker points on the F18 phantom and the corresponding area on the distorted images. We assumed that the mapping area on the distorted image is quadrilateral, which may introduce uncertainties in the distortion corrections since a quadrangle may not have a quadrilateral image due to gradient

distortion and non-uniformity of the main magnetic field. However, the quadrilateral approach is a reasonable one since it will provide the required accuracy for our application.

Based on the quadrilateral approach, we can perform the point-by-point correction to the distorted images. First, those pixels inside the area defined by any four markers on the phantom image are correlated with these on the distorted image by a linear mapping. This is done by equally dividing the distance between any two points on both images and then correlating the areas defined by the connecting lines.

The area (distorted pixels) on the distorted image may be larger or smaller than the area (pixels) on the F18 phantom. Figure 3 shows a distorted pixel and its relationship with pixels on the distorted MR image. Assume that a pixel (m,n) on the F18 phantom has its corresponding distorted area on the MR image that is larger than the MR pixel size as shown in figure 3. The area covers not only the pixel (i,j) but also part of pixels $(i-1,j)$, $(i,j-1)$, $(i,j+1)$, $(i+1,j+1)$ and $(i+1,j)$. The overlapping areas here are represented by $\Delta(k,l)$ with $k=i-1,i,i+1$ and $l=j-1,j,j+1$. Then, the corrected intensity value for pixel (m,n) can be calculated as:

$$I(m,n) = \frac{1}{S} \sum_{k,l} \Delta(k,l) \cdot I'(k,l) \tag{3}$$

where, $k=i-1,i,i+1$ and $l=j-1,j,j+1$, S represents the value of the area (m,n) and $I'(k,l)$ is the image intensity for pixel (k,l) on the distorted MR image. If the distorted area of a pixel is smaller than the size of a pixel, the image intensity can be approximated by choosing $I(m,n)=I'(k,l)$.

2.4. Evaluation of the point-by-point distortion correction method

Since there is no patient-induced distortion for the 0.23 T MR unit with the sequences used in our study, the distortion maps derived from the phantom measurement can be used to correct the residual MR distortions. However, detailed testing on real patients must be performed before its clinical implementation. In this work, distortion-free CT images were used to compare with MRI images of prostate patients before and after the GDC corrections.

It was understood that the differences between the CT and MRI external contours for the same patients resulted not only from MR image distortions but also from setup uncertainties between CT and MR scans, which had to be minimized or excluded in order to evaluate the accuracy of the distortion correction. As previous investigators reported (Mah et al 2002, Chen et al 2005), the setup uncertainties in CT and MR could be about 0.5 cm respectively. The combined setup uncertainties in our CT and MRI comparisons were therefore expected to be ~ 0.7 cm (one standard deviation). Clinically, we have observed setup uncertainties between CT and MR scans larger than 1 cm for some patients with large lateral dimensions.

In order to evaluate our point-by-point distortion correction method, static, porcine tissue samples were used in this study to eliminate the setup uncertainties. We imaged frozen, porcine leg quarters on our CT and MRI scanners and arranged a pair of these to mimic human pelvis, using a special cradle to hold their positions firmly. All the MR images were scanned with our routine clinical 3-dimensinal fast spin echo sequences (3DFSE, 256 x 256, 1.95 mm pixel, 3 mm slice thickness, TR = 3000 ms, TE = 140 ms, BW readout gradient > 100 Hz/pixel), and a standard FOV of 48 cm. The external contours from the CT images were exported to the MR images after fusion for direct comparison.

3. Results and discussion

Figure 4a shows the actual viewable areas of our 0.23 T MR unit for a standard 48 cm FOV for prostate imaging that indicate the geometrical limitations of the scanner at different transverse planes. The marker points outside the viewable areas were outside the 256 by 256 matrix due to the MR geometric distortions and were lost in the initial raw MR images. The GDC software reduced the MR geometric distortions significantly but could not recover the missing marker points. The outer contour in figure 4a represents the actual viewable area of the scanner at the isocenter transverse plane and the inner contour represents the actual viewable area that is 10 cm away from the isocenter. Any transverse planes within 10 cm of the isocenter will have a viewable area between the two contours. The actual viewable area decreases with increasing distances from the isocenter, which is expected because of the loss of uniformity of the magnetic field at large distances. The distortion maps were established for every transverse plane along the I-S direction with a 0.5 cm interval and the maps were used to correct the distortions in our point-by-point distortion correction method. Figure 4b shows the distortion map of a transverse plane at the location of the scanner's center. Compared with the physical pattern of the F18 phantom, the residual distortions after the GDC can be observed and the maximum distortion is about 1 cm.

Figure 5 shows MR images of the F18 phantom with and without the GDC post-processing and after the point-by-point corrections. These images were taken at the center of the scanner with a standard FOV of 48 cm for prostate imaging. We then established a new effective FOV based on the viewable area for this transverse plane, which showed clinically insignificant distortions after the point-by-point correction. We established the effective FOVs for all the transverse planes in the same way. For later routine clinical applications, only the image points within the effective FOVs were processed. The maximum distortions were about 1.0 cm before the point-by-point correction and it was reduced to <0.3 cm after the correction. The improvement on the marker positions is shown clearly.

A few patients were selected and processed to test our method. We found that the distortions were reduced dramatically after applying the GDC and our point-by-point corrections. Figure 6 shows a distortion-free CT image with an external contour drawn by a physician and two MR images with and without the GDC and a MR image with both the GDC and the point-by-point distortion correction. The maximum residual error after our point-by-point distortion correction is expected to be ~0.3 cm based on the investigation results using the F18 phantom (up to 2 cm distortions were corrected compared with the initial image). From figure 6d, the differences between the CT external contour and the distortion corrected image are still seen. It was believed that the major reason for these differences was the setup uncertainty between the CT and MR scans.

To demonstrate this, we performed paired CT and MR scans for large, static porcine samples immobilized in a specially made cradle. Figure 7a shows a distortion-free CT image of the porcine samples, which were 42 cm in lateral dimensions. The external contour of the CT image was transferred to the MR images for comparison. The maximum distortion measured on the initial MR image was 2.1 cm (figure 7b) and significant residual distortions were still observable after the DGC post-processing (figure 7c). Measurements on the final MR image showed that the MR geometrical distortions were reduced to < 0.3 cm after our point-by-point distortion correction (figure 7d).

4. Conclusions

In this paper, we have described our work on MR image distortion correction to further improve the accuracy of dose calculation for MR based treatment planning for prostate cancer. Our goal was to develop practical methods for the clinical implementation of MRI based treatment planning. Our studies showed that, with our routine clinical 3-dimensinal fast spin echo sequences (3DFSE, 256 x 256, 1.855 mm pixel, TR = 140 ms, TE = 3000 ms, BW readout

gradient > 100 Hz/pixel), there was no patient-induced distortions. Therefore, the residual machine specific geometrical distortions after the GDC could be quantified by phantom measurements and further reduced by our point-by-point correction technique. The effective FOVs of the scanner were established based on the actual viewable areas with adequate geometric distortion corrections (ensuring < 5 mm distortion error). The effective FOV for prostate imaging using a standard FOV of 48 cm has been expanded from 36 cm using the existing GDC software to 42 cm using the point-by-point distortion correction technique developed in this work. Our results indicated that, with the distortion maps established in this work, we could correct MR geometrical distortions for patients of lateral dimensions up to 42 cm. Significant improvement in dose calculation has been achieved based on a 1-2 cm improvement in patient external contour determination.

Acknowledgements

References

Beavis AW, Gibbs P, Dealey RA and Whitton VJ 1998 Radiotherapy treatment planning of brain tumours using MRI alone Br *J Radiol.* **71**(845):544-8

Chang H and Fitzpatrick JM 1990 Geometrical image transformation to compensate for MRI distortions, *In SPIE* Vol. **1233** Medical Imaging IV: Image Processing

Chen L, J. Zhu et al 2005 Image Guided Radiation Therapy: Investigation of Interfraction Setup and External Contour Variation for Prostate IMRT Using CT and MRI. Abstract for 2005 AAPM annual meeting

Chen L, Li J, Mah D, Ma CM, Wang L, Ding M, Freedman G, Movsas B and Pollack A 2002 Monte Carlo investigation of dosimetry accuracy for MR-based treatment planning. *Med. Phys.* **29**(6) 1339 (abstract)

Chen L, Price RA Jr., Li J et al 2003 Evaluation of MRI-based treatment planning for prostate cancer using a commercial TPS *Med. Phys.* Vol. **30**, no. 6, P1507

Chen L, Price RA Jr et al 2004a MRI-based Treatment Planning for Radiotherapy: Dosimetric Verification for Prostate IMRT, *Int. J. Radiation Oncology Bio. Phys.* Vol.**60**, No.**2**, pp. 636-647

Chen L, Price RA Jr, et al 2004b Dosimetric Evaluation of MRI-based Treatment Planning for Prostate Cancer, *Phys. Med. Biol.* **49** 5157-5170.

Chen Z, Ma C-M et al 2004c Investigation of CT-MR Image Intensity Correlation for MRI-based Dose calculation. *Med. Phys.*, Vol.**31** No. **6** (abstract)

Debois M, Oyen R, Maes F, Verswijvel G, Gatti G, Bosmans H, Feron M, Bellon E, Kutcher G, Van Poppel H and Vanuytsel L 1999 The contribution of magnetic resonance imaging to the three-dimensional treatment planning of localized prostate cancer *Int J Radiat. Oncol. Biol. Phys.* **45**:857-65

Fransson A, Andreo P, Potter R 2001 Aspects of MR image distortions in radiotherapy treatment planning. *Strahlenther Onkol* **177**: 59-73

Guo WY 1998 Application of MR in Stereotactic Radiosurgery *J. Magn. Res. Imag.,* 8, 415-420

Hanks GE 1999 Progress in 3D conformal radiation treatment of prostate cancer. *Acta. Oncol.* **38** (Suppl 13):69-74

Hanks GE, Hanlon AL, Schultheiss TE et al 1998 Dose escalation with 3D conformal treatment: five year outcomes, treatment optimization and future directions. *Int J. Radiat. Oncol. Biol. Phys.* **41**:501-510

Khoo VS, Adams EJ, Saran F, Bedford JL, Perks JR, Warrington AP and Brada M 1999 A comparison of MRI and CT for the radiotherapy planning of prostate cancer: a feasible study *The British Journal of Radiology* **72**:1309-17

Kondziolka D, Dempsey PK, Lunsford LD, Kestle JRW, Dolan EJ, Kanal E and Tasker RR 1992 A comparison between magnetic resonance imaging and computed tomography for stereotactic coordinate determination. *Neurosurgery*, **30**:402--407

Lee YK and Bollet M, 2003 Radiation Treatment Planning of Prostate Cancer Using Magnetic Resonance Imaging Alone, *Radiotherapy and Oncology* **66**:203-216

Mah D, Michael Hanlon SA, Freedman G, Milestone B, Mitra R, Shukla H, Movsas B, Horwitz E, Vaisanen PP and Hanks GE 2002 MRI Simulation: Effect of gradient distortions on three-dimensional prostate cancer plans *Int. J. Radiat. Oncol. Biol. Phys* **53**:757-765

Michiels J, Bosmans H, Pelgrims P, Vandermeulen D, Gybels J, Marchal G and Suetens P 1994 On the problem of geometric distortion in magnetic resonance images for stereotactic neurosurgery. *Magnetic Resonance Imaging*, **12(5)**

Pollack A, Zagars GK and Rosen II 1999 Prostate cancer treatment with radiotherapy: maturing methods that minimize morbidity. *Semin. Oncol.* **26**:150-161

Pollack A, Zagars GK, Smith LG, Lee JJ, von Eschenbach AC, Antolak JA, Starkschall G and Rosen I 2000 Preliminary results of a randomized radiotherapy dose-escalation study comparing 70 Gy with 78 Gy for prostate cancer. *Journal of Clinical Oncology* **18(23):**3304-3911

Philips 2003 Radiation Therapy Support Kit , Instruction for use, Release 4.0.2

Photon Treatment Planning Collaborative Working Group 1991 Role of inhomogeneity corrections in three-dimensional photon treatment planning *Int J Radiat Oncol Biol Phys* **21**:59-69

Rasch C, Barillot I, Remeijer P, Touw A, van Herk M, Lebesque JV 1999 Definition of the prostate in CT and MRI: a multi-observer study. *Int J Radiat Oncol Biol Phys* **43**:57-66

Roach M 3rd, Faillace-Akazawa P, Malfatti C, Holland J, Hricak H 1996 prostate volumes defined by magnetic resonance imaging and computerized topographic scans for three-dimensional conformal radiotherapy. *Int J Radiat Oncol Biol Phys* **35**: 1011-1018

Schad LR, Boesecke R, Schlegel, Gunther W, Hartmann H, Sturm V, Strauss LG and Lorenz W 1987 Three dimensional image correlation of CT, MR, and PET studies in radiotherapy treatment planning of brain tumors. *Journal of Computer Assisted Tomography*, **11(6)**:948--954

Sumanaweera T, Glover G, Song S, Adler J and S. Napel 1994 Quantifying MRI geometric distortion in tissue. *Magnetic Resonance in Medicine*, **31**

Zelefsky MJ, Leibel SA, Gaudin PB et al 1998, Dose escalation with three-dimensional conformal radiation therapy affects the outcome in prostate cancer. *Int J Radiat Oncol Biol Phys*. **41**:491-500

Figure Captions

Figure 1. The Philips 0.23 Tesla open MR unit (a) and the F18 phantom (b). The F18 phantom with the support structure is placed in the body/spine coil. The support structure allows the marker plane to align with any selected imaging planes.

Figure 2. A diagram showing the mapping of the pixels between the distorted image and the F18 phantom.

Figure 3. A diagram to illustrate the pixel intensity calculation.

Figure 4. Actual viewable areas of the scanner and a distortion map. (a) The outer contour represents the viewable area of the transverse plane at the isocenter of the scanner and the inner contour the viewable area at the transverse planes 10 cm away from the isocenter plane along the I-S direction. The viewable areas for any transverse planes within 10 cm of the isocenter will be between the two contours. (b) A distortion map measured based on the F18 phantom measurement. Without distortion, any adjacent marker points laterally and vertically would have a 2.5 cm separation.

Figure 5. MR images of the F18 phantom at the isocentric plane: (a) before the GDC, (b) after the GDC, and (c) further corrected by the point-by-point distortion correction.

Figure 6. CT and MR images of a prostate patient: (a) a distortion-free CT image, b) the same patient imaged on the MR scanner without any distortion corrections, c) only with the GDC post-processing, and d) with both the GDC and our point-by-point correction. The external contours on the MR images were exported from the CT image after image fusion.

Figure 7. CT and MR images of frozen porcine samples: (a) a distortion-free CT image at the isocentric plane, (b) the same isocentric slice imaged on the MR scanner without any distortion corrections, (c) only with the GDC post-processing, and (d) with both the GDC and our point-by-point correction. The external contours on the MR images were exported from the CT image after image fusion.

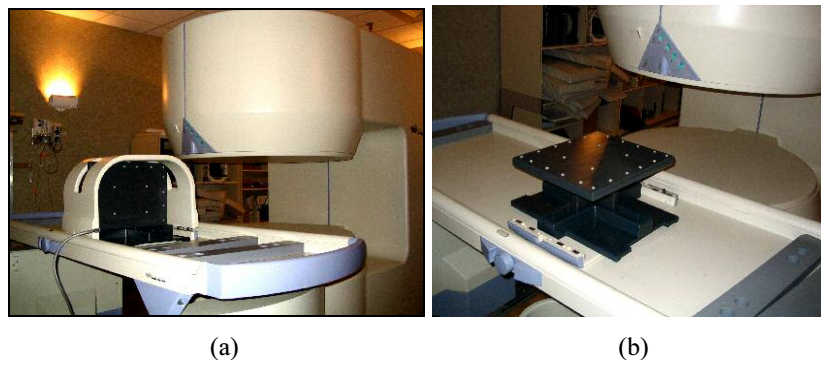(a)   (b)

Figure 1. The Philips 0.23 Tesla open MR unit (a) and the F18 phantom (b). The F18 phantom with the support structure is placed in the body/spine coil. The support structure allows the marker plane to align with any selected imaging planes.
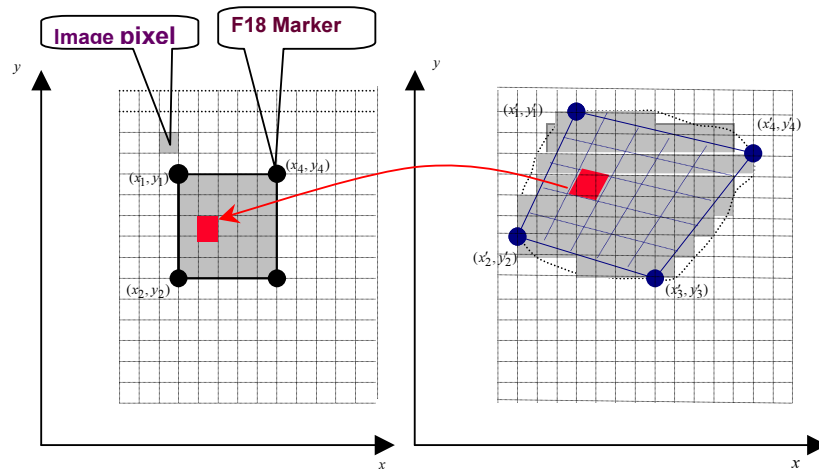
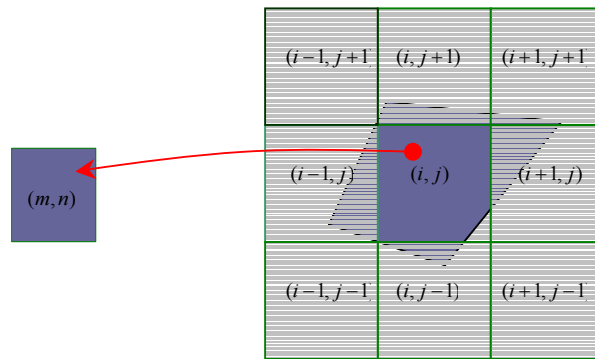Figure 2. A diagram showing the mapping of the pixels between the distorted image and the F18 phantom.

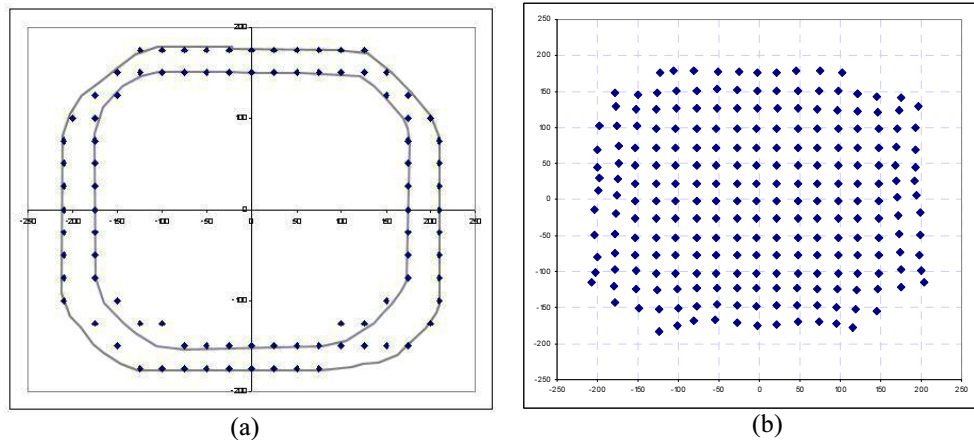Figure 3. A diagram to illustrate the pixel intensity calculation.

(a)

(b)

Figure 4. Actual viewable areas of the scanner and a distortion map. (a) The outer contour represents the viewable area of the transverse plane at the isocenter of the scanner and the inner contour the viewable area at the transverse planes 10 cm away from the isocenter plane along the I-S direction. The viewable areas for any transverse planes within 10 cm of the isocenter will be between the two contours. (b) A distortion map measured based on the F18 phantom measurement. Without distortion, any adjacent marker points laterally and vertically would have a 2.5 cm separation.
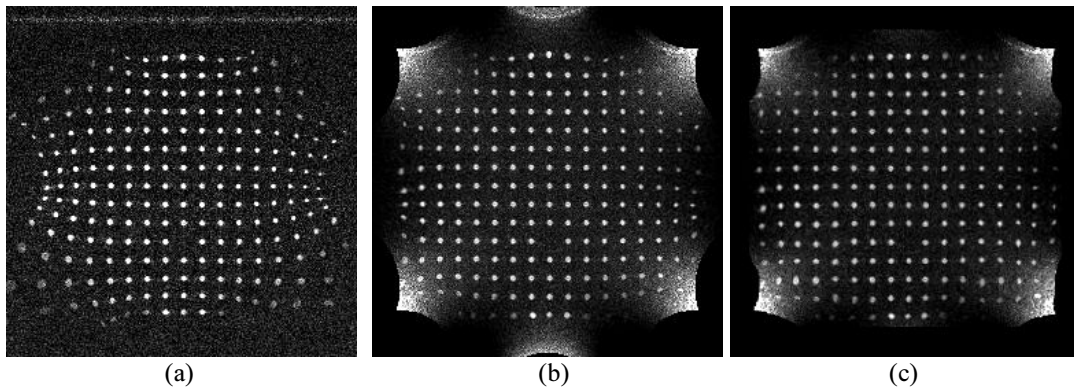
(a)   (b)   (c)

Figure 5. MR images of the F18 phantom at the isocentric plane: (a) before the GDC, (b) after the GDC, and (c) further corrected by the point-by-point distortion correction.
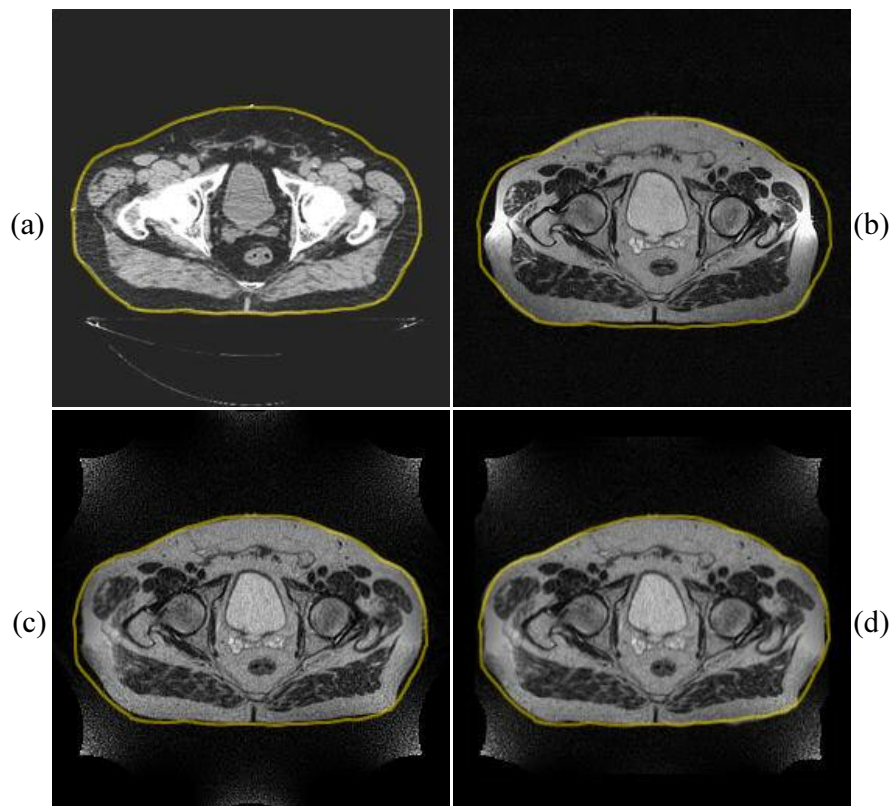
Figure 6. CT and MR images of a prostate patient: (a) a distortion-free CT image, b) the same patient imaged on the MR scanner without any distortion corrections, c) only with the GDC post-processing, and d) with both the GDC and our point-by-point correction. The external contours on the MR images were exported from the CT image after image fusion.
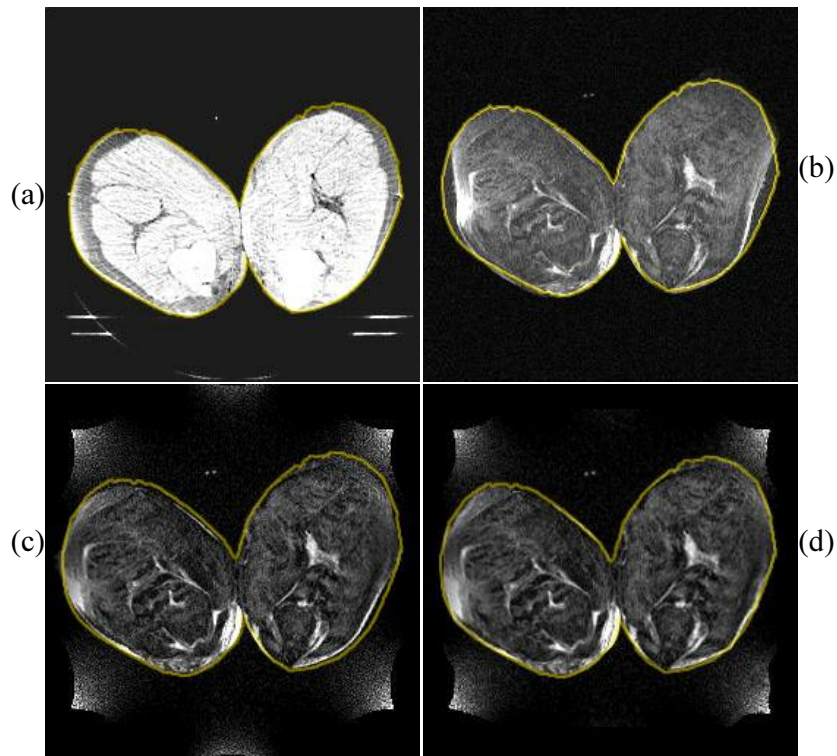
Figure 7. CT and MR images of frozen porcine samples: (a) a distortion-free CT image at the isocentric plane, (b) the same isocentric slice imaged on the MR scanner without any distortion corrections, (c) only with the GDC post-processing, and (d) with both the GDC and our point-by-point correction. The external contours on the MR images were exported from the CT image after image fusion.

Monte Carlo dose verification of MR image based IMRT treatment planning for prostate cancer

Z. Chen, C-M Ma, J. Yang, J. Li, W. Luo, J. Fan, K. A. Paskalev, R. A. Price Jr, Y. Chen and L. Chen,

Department of Radiation Oncology, Fox Chase Cancer Center, Philadelphia, Pennsylvania, 19111

E-mail: jay.chen@fccc.edu

Abstract

In this work, we used the Monte Carlo method to verify dosimetric accuracy and consistency for MR based IMRT treatment planning for prostate cancer. Selected patients were scanned on both a CT simulator and a 0.23 T open MR scanner and IMRT plans were generated on Corvus for these patients based on CT data. Monte Carlo simulations were then performed for these plans using homogeneous geometry based on CT and MRI, and heterogeneous geometry built based on CT numbers or different bulk densities for MR contoured bony structures. The homogenous density was chosen as 1.0g/cm^3 and the densities of bones were chosen in the range $1.5 - 2.2 \text{ g/cm}^3$. Isodose distributions and dose-volume histograms (DVH) were used in the plan comparison. For IMRT treatments with all the beams arranged in an axial plane, the mean dose values of the CTV for homogeneous geometry based on CT were about 2% higher than those for heterogeneous geometry based on CT. The difference in the mean CTV dose between homogenous MRI and heterogeneous CT geometries was about 3% and less. The DVH curves also agreed to within 5% in dose or volume among these plans. For treatments with larger discrepancies found in the CTV dose between homogeneous geometry and heterogeneous geometry due to the significant attenuation of the oblique beams going through the femurs, bulk-

density assignment to femurs and femoral heads were used and a 1.8g/cm3 optimal bulk-density was found to reduced the discrepancies from 10% to less than 3% in MR-based planning.

Keywords: MRI-based treatment planning, IMRT, Monte Carlo, Dose calculation.

1. Introduction

Intensity modulated radiation therapy (IMRT) is considered an advanced technique for radiation therapy and has received widespread acceptance. Because the ratio of normal tissue dose to tumor dose can be further reduced with IMRT, higher and more effective radiation doses can be delivered safely to tumors with fewer side effects as compared with conventional radiotherapy techniques. In our department, over 2 thousand prostate cancer patients have been treated with IMRT over the past few years to improve local tumor control and to reduce normal tissue complications. However, as dose levels are increased with IMRT, accurate target delineation and dose calculation become crucial. As we know, magnetic resonance image (MRI) provides superior image quality for soft-tissue delineation compared with computed tomography (CT) (Khoo et al 2000, Tanner at al 2000, Potter et al 1999). For example, 30% to 40% improvement in target volume delineation for prostate treatment could be achieved by using MRI instead of CT in treatment planning (Krempien at al 2002, Debois et al 1999). Because of the superior soft-tissue contrast from MRI, CT and MRI fusion has been used extensively clinically in IMRT to ensure both accurate anatomical delineation and dose calculation for radiotherapy of prostate cancer.

Although CT and MR fusion has been widely accepted as a practical approach for both accurate delineation (using MR data) and dose calculation (using CT data) it would be ideal if MRI could

replace CT entirely for treatment planning, which will retain the superior soft tissue contrast for image segmentation and at the same time eliminate the potential errors in image fusion due to variations in patient setups between CT and MR scans and the uncertainties in target localization between the two image modalities. Furthermore, MRI based treatment planning will avoid redundant CT imaging sessions, which in turn will avoid unnecessary radiation exposure to patients, reduce treatment costs, and save patient, staff and machine time. Even through there are a few technical challenges in MRI-based treatment planning, such as the lack of electron density information and geometrical distortions, there have been growing interests in the utilization of MRI based radiotherapy treatment planning since the past decade, and progress has been made in developing an effective MRI based method for treatment planning (Michiels et al 1994, Beavis et al 1998, Guo 1998, Mah et al 2002, Chen et al 2002, Chen et al 2003, Lee et at 2003).

In our department, dose calculation in IMRT treatment planning for prostate cancer is usually performed without heterogeneity correction even in our CT-based planning because of the following considerations: 1) the target is surrounded by soft tissues and it has been common practice to use homogenous geometry for dose calculation in the pelvic region; 2) the use of contrast agent in imaging sometimes changes the CT numbers in the bladder significantly and the changes in electron density in the bladder will affect the dose in the target and other organs significantly if heterogeneity corrections are applied; 3) large gas pockets occasionally accrued in the rectum on the planning images may affect the dose distribution and/or MU calculation significantly when heterogeneity correction is used but they may have little effect on the dose delivered since the gas pockets may not appear again in the subsequent treatments. Based on the considerations above, homogeneous geometry is used to avoid these problems in the treatment planning for the routine treatment. Since the homogenous geometry approach in dose calculation for prostate cancer treatment planning is a common and practical choice clinically, the lack of electron density information in MRI-based treatment planning will no longer be a critical

problem. MRI-based treatment planning can be used to achieve more accurate dose delivery due to better target and internal organ delineation and localization from MR images. However, the geometrical distortions on MR images must be quantified and corrected before MRI-based treatment planning is used clinically. We have developed an efficient method to quantify and correct the machine induced geometrical distortions to less than 0.3 cm (Chen et al, 2004b). The patient induced geometrical distortions have been eliminated by choosing high bandwidth of the pulse sequences (> 100 Hz/pixel) in frequency encoding direction (Fransson et al 2001). In this study, all the MR images of patients used for dose calculation have been corrected for geometrical distortion and the residual distortions after the correction were less than 0.3 cm.

In IMRT planning, the accuracy of dose calculation is also a particular concern, especially for the high dose-gradient regions generated by small beamlets. There are different algorithms used by commercial planning systems for IMRT dose calculation (Bourland and Chaney 1992, Ostapiak et al 1997, Mackie at al 1985, Boyer and Mok 1985, Ahnejo 1989, Battista and Sharpe 1992, Woo and Cunningham 1998). All these algorithms employ some approximations in dose calculation, which can affect the final dose results (Mohan 1997, Ma at al 1999, Ma et al2000). In modern radiation therapy, the Monte Carlo dose calculation algorithm has been demonstrated as the most accurate method (Rogers and Bielajew 1990, Mohan 1997). In this work, all of the dose calculations were performed using our Monte Carlo treatment planning system to investigate inhomogeneity effect in the CT-based calculation and to compare the CT results with bulk-density assignment in MR-based calculations. Another reason of choosing Monte Carlo simulation for this study was the flexibility of imaging processing on our Monte Carlo system. For most of our clinical plans, the CT and MR data were acquired with different fields of views (FOV) and different voxel sizes (CT: 512 x 512; MR 256 x 256) and the differences in FOV and voxel size resulted in discrepancies in structure volumes and uncertainties in dose calculations, which affected the final dose distributions (Chen et al 2004). The flexibility of imaging

processing on our Monte Carlo system allowed us to pre-process the CT and MR data sets so that the two data sets could have the same FOV, voxel size and the same RT structure volumes to avoid these unnecessary discrepancies.

For MR-based treatment planning with uniform geometry, optimal beam arrangement becomes more important since heterogeneity effect may be significant if many beams are arranged penetrating through bony structures in the pelvic area. For most of the prostate patients treated in our department with IMRT, the clinical requirements (target coverage and conformity, constraint on the dose to critical organs) can be achieved with co-planar beams arranged in AP, AP oblique, PA oblique (only soft tissues irradiated) and two lateral directions (two femoral heads are irradiated). The inhomogeneity effect in this beam arrangement has been shown to be clinically insignificant. However, for some special cases with non-coplanar beam arrangements, it is necessary to allow more beams penetrating through bony structures in order to meet the clinical requirement, which increases the heterogeneity effect on the dose distribution.

In this work, patient-specific Monte Carlo dose calculations based on MR data and CT data were performed using the source model established for Primus linear accelerator (Siemens Medical Solution, Concord, CA). The results predicted by MR-based calculations were compared to the results predicted by CT-based calculations using the same setup parameters and leaf sequencing files taken from these patient's actual treatment plans on Corvus. For clinical cases with non-coplanar beam arrangements where a large amount of pelvic bones were irradiated in the treatment, bulk-densities were assigned to the femurs and femoral heads in MR-based calculations to reduce the inhomogeneity effect.

2. Materials and method

2.1 IMRT planning

The images for all the patients in this work were acquired on a Picker AcQSim CT scanner and a Philips MR 0.23 T open scanner (Philips Medical System, Cleveland, OH). Target and critical structures were delineated by the physicians based on the fused CT and MR images using the AcQSim VoxelQ segmentation tools. The segmented CT scans were transferred to the treatment planning system for IMRT planning. The IMRT plans were then generated on the Corvus inverse-planning system (Version 5) based on the CT data (Nomos Corp. Sewickley, PA). Once the plan was approved by the physician, it was moved to our Monte Carlo system with the patient's CT and contour data, treatment isocenter, leaf-sequencing files and beam parameters for dose calculation. On the Monte Carlo treatment planning system, images were further processed so that the FOV, voxel size and volumes of RT structures were kept the same for both CT-based and MR-based dose calculations.

2.2 Monte Carlo dose calculation

The Monte Carlo Method is known as the most accurate dose calculation method for radiotherapy. The Monte Carlo code used in this work for dose calculation was MCSIM, which is an EGS4/PRESTA user code developed at Fox chase Cancer Center (FCCC) (Ma et al 2002b, 2004). The beam information was represented using a source model, which was built based on measured beam data (Jiang et al 2000, 2001; Yang et al 2004), and validated for Monte Carlo dose calculation for photon beams from our Siemens accelerators. During the calculation, the multi-leaf collimator leakage effect was taken into account when intensity maps were reconstructed from a plan. The accuracy of the dose calculation is better than 2% compared with measured data (Li et al 2002, Ma et al 2001). For each patient, an RTP file from the Corvus treatment planning system that includes patient setup parameters and beam and leaf-sequence information was used for the Monte Carlo dose calculation. For the Monte Carlo simulation, the electron and photon energy cutoffs, ECUT and PCUT, for particle transport were set to 700 keV and 10 keV, respectively. The energy thresholds for δ ray production (AE) and for

Bremsstrahlung production (AP) were also set to 700 keV and 10 keV, respectively. The maximum fractional energy loss per electron step (ESTEP) was set to 0.04 and the default parameters were used for the PRESTA algorithm.

The patient geometry used for the Monte Carlo calculations was created based on both CT and MR data. The materials and mass densities of CT based geometries were converted from the CT numbers based on a piecewise linear conversion curve that was given by Ma et al (1999).

Seventy million particle histories were used in the Monte Carlo simulations to archive less than 0.5% statistical uncertainties to the target dose for all the IMRT plans. Each photon was split 20 times to improve the simulation efficiency using the photon-splitting technique implemented in MCSIM.

2.3 Investigation of inhomogeneity effect for MR-based calculation

CT-based IMRT Monte Carlo dose calculations with and without heterogeneity correction were performed for each selected plan in order to investigate heterogeneity effect caused by different beam angle arrangements. Based on the results, MR-based IMRT dose calculations were then performed to the plan using either uniform density geometry or uniform density geometry with bulk electron density assigned to bony structures. For the plans with insignificant inhomogeneity effect, uniform geometries with water density were used in the MR-based dose calculation. For the plans that bony structure constitutes a large part of volume irradiated, uniform density geometry with bulk electron density assigned to bony structures was used in the MR-based dose calculation.

2.4 Dose verification of MR-based plan

The differences in isodose distributions and dose-volume histograms (DVH) were used to compare the results of the CT-based and the MR-based dose calculations for each IMRT plan. The clinical target volume (CTV) was chosen for the dose-volume comparison. Clinical quantities such as the mean dose, maximum and minimum dose received by the CTV and the critical structures were compared. The maximum dose was defined as the highest dose received by 1% of the target volume and the minimum dose was defined as the lowest dose received by 99% of the target volume, respectively. Other parameters such as the dose at the isocenter and the dose received by 95% and 5% of the CTV were also compared.

The paired CT and MR data for any patients in this work were pre-processed to have the same pixel resolution. The internal contours of the targets and critical organs were contoured by physicians on the fused CT-MR images. A special computer code was developed to convert the patient CT and MR image data from the DICOM format to geometries specially formatted for the MCSIM code.

3. Results and discussion

With proper geometrical distortion corrections for the MR images and the use of uniform water equivalent density geometry in the dose calculations, it was expected that the IMRT plans based on CT and MR data would agree well. Figure 1 shows the DVH curves from the CT and MR-based dose calculations for one of the 10 IMRT plans investigated. This IMRT plan used 10 MV photon beams with 9 gantry angles on a Siemens Primus accelerator with 39 fractions to deliver 78 Gy. The difference in the mean dose of the CTV was 0.3% between the CT-based and MR-based calculations. The differences in the maximum dose and in the minimum dose of the CTV were 0.8% and 0.2% respectively. Figure 2 shows the isodose distributions from the CT- and

MR-based calculations for this patient. The isodose distributions for both the CT- and MR-based plans are similar and the differences in the DVH are clinically insignificant.

Table 1 lists the results of the dose calculations using MR data and CT data with homogeneous water equivalent geometries for 10 IMRT prostate plans. The data presented in Table 1 were calculated as the percentage differences between CT-based and MR-based results, i.e., $(D_{CT} - D_{MR})/D_{MR} \times 100\%$, where D_{CT} is the dose from CT-based calculation and D_{MR} is the dose predicted by MR-based calculation. ΔD_{min} is the difference in the minimum dose of the target, ΔD_{mean} is the difference in the averaged target dose, ΔD_{max} is the difference in the maximum target dose, and ΔD_5 and ΔD_{95} are the differences of the dose received by 5% and 95% of the target volume, respectively. The average differences over the 10 IMRT plans for the clinical quantities used in the comparison were all less them 1.5%.

Our preliminary results demonstrated that MR-based planning was equally good as CT-based planning for prostate cancer with homogeneity geometry in the dose calculation. The differences between CT and MR-based calculations showed in table 1 mainly came from the setup uncertainties in the CT and MR image acquisition (Chen et al 2005). The beam arrangements of the 10 IMRT plans were all commonly used for routine treatment at Fox Chase Cancer Center: 1) one anterior, 2) two or four anterior oblique, 3) two lateral and 4) two or four posterior oblique beams. The couch angles were set as zeros in all the plans (i.e. coplanar beam arrangements). Table 2 shows the differences of the clinical quantities between MR-based dose calculations with uniform water equivalent geometry and CT-based dose calculations with heterogeneity correction. The maximum differences were less than 4% and the averaged differences over the 10 IMRT plans were less then 1.6% for all the quantities in the comparison, indicating that the uniform geometry was a good approach with our commonly used beam arrangements. These results were consistent with previous findings (Chen at al 2004 and Yang J et al 2004).

However, for some clinical cases non-coplanar beam arrangements where a large amount of pelvic bones were irradiated in the treatment, heterogeneity correction became necessary in planning. Figure 3 shows a comparison of DVHs for a CT-based IMRT plan with and without heterogeneity correction, More than 8% differences in dose calculations were observed. The 7-field plan was generated with special clinical requirements and several non-coplanar beams were arranged to achieve better target dose coverage and rectal sparing. Table 3 lists the orientations of the beams and the dose contributions from each of the 7 beams with and without heterogeneity correction. More than 10% differences were found in the single beam calculations for some beams going through a large amount of pelvic bones.

To utilize MR-based planning for the treatments with large amount of pelvic bones irradiated, inhomogeneity corrections must be taking into account and bulk-density assignment to bony structures was proposed since there is no simple point-to-point correlation between MR signal intensities and electron densities of the materials imaged (Young Lee 2003). Various bulk-density assignments to the femurs and femoral heads were studies in this work. Figure 4 shows the changes in the DVH with different bulk density assigned to the femurs (between 1.5 and 2.2 g/cm^3) for two IMRT plans with large amount of pelvic bones irradiated. Table 4 shows the target doses based on CT data with heterogeneity correction and based on MR data with bulk densities assigned to the femurs and femoral heads for the two IMRT plans. It is clear that $1.8 g/cm^3$ is the optimal value for the bulk-density assignment.

The IMRT plan showed in table 3 was re-calculated using MR data with $1.8 \ g/cm^3$ bulk-density assigned to the femurs and femoral heads and the results are listed in table 5. The averaged target doses for each beam as calculated using CT data with heterogeneous correction and using MR data with bulk-density assignment agreed well compared with CT uniform water equivalent

geometry (see table 3 and 5). For those beams with gantry/table angles as 275/340, 85/20 and 85/0, the differences in the average target doses were decreased from about 10% with uniform water equivalent geometry to about 3% or less after using $1.8 g/cm^3$ bulk density assignment to femurs and femoral heads. The changes in DVHs using CT data with $1.8 g/cm^3$ bulk density for the femurs and femoral heads also confirmed our findings (see fig 4a).

Even though $1.8 g/cm^3$ bulk-density assignment gave the best fit in our dose calculation for MR-based planning for prostate cancer, it should be pointed out that the optimal bulk-density assignment only reflects the overall inhomogeneity effect caused by the bones in the pelvic region. The optimal value of bulk-density that reduces the inhomogeneity effect at the pelvic region may vary slightly with the energy of the beams and the way the contours of pelvic bones were drawn by physicians. The values of $1.8 g/cm^3$ for optimal bulk-density assignment for the femurs and femoral heads were obtained based on the results of our calculations only. We have used different bulk-density assignments in the dose calculations for IMRT plans, 4 beam conformal plans and single beams with different incident angles and compared the results with those predicted by CT data with heterogeneity corrections; $1.8 g/cm^3$ gave the best fit. Figure 5 shows how the differences of the isodose distributions between CT and MR calculation with and without $1.8 g/cm^3$ bulk-density assignment. Table 6 shows the changes of using $1.8 g/cm^3$ bulk-density assignment in the dose calculation for 5 patients with a single 6 MV or 18 MV beam, 10 x 10 cm field size with gantry/table angles of 270/340 degrees. Improvement on the effect of inhomogeneity can be easily seen from the results of using $1.8 g/cm^3$ bulk-density.

For critical organs in prostate treatment, such as rectum and bladder, the dose differences between CT- and MR-based calculations were negligible compared with the differences in the target dose

for all the plans studied (see figures 1, 3 and 4). The results are not presented here since the differences from these calculations were clinically insignificant.

4. Summary

In this work, we have used the Monte Carlo method to validate the dose accuracy and consistency for MR-based treatment planning of prostate cancer. The results were compared with CT-based dose calculations (with and without inhomogeneity correction) for plans with different beam arrangements used in routine clinical treatment.

We found that the differences in the results between CT data (with heterogeneity correction) and MR data (with uniform water equivalent geometry) were about 3% or less and less than 2% in the mean values for the 10 plans with beams arranged in one axial plane (see table 2). For MR-based calculations (with homogeneous geometry), our results demonstrated that the differences between MR-based calculations and CT-based calculations (without heterogeneity correction) were less than 2% for the individual patients and about 1% in the mean values, which proved that MR-based IMRT plans can be used to replace CT-based planning clinically (see table 1). The 1% - 2% differences in dose calculations were mainly caused by the setup uncertainties of the two imaging modalities if geometrical distortions on the MR images were corrected to less than 3 mm.

For treatments in which relatively large amount of bones are irradiated, MR-based treatment planning with homogeneous geometry would not be appropriate because of the excessive attenuation of the photon beams passing through bony structures. However, by assigning bulk densities to the bony structures especially for the femurs and femoral heads, the dose differences could be reduced to less than 3% (see table 3, 4 5 and 6). The bulk densities assigned to the

femurs that gave the best fits to CT-based calculations with heterogeneity correction were $1.8 g/cm^3$ in our simulations.

We have established a practical procedure for MR-based treatment planning, in which MR geometrical distortions are properly corrected, a useful DRR technique is developed/implemented and homogeneous geometry is used in the dose calculation. Our results show that it is accurate and consistent in dose calculation for prostate cancer treatment. In our department, one third of radiotherapy treatments are for prostate cancer and homogeneous geometry has been used in prostate planning dose calculation. By using MR-based treatment planning the savings in staff time, patient time and treatment costs would be significant and the additional radiation exposure from CT scans can be avoided. It is concluded that MR-based radiotherapy treatment planning can be widely utilized clinically for prostate cancer treatment. Further investigations are carried out for other sites where heterogeneity effect is not significant.

References

Ahnejo A 1989 Collapsed cone convolution of radiant energy for photon dose calculation in heterogeneity media *Med. Phys*. **16** 577-92.

Battista J J and Sharpe M B1992 True three dimensional dose computations for megavoltage x ray therapy: a role for superposition principle *Austral. Phys. Eng. Sci. Med.* **15** 159-78.

Beavis AW, Gibbs P, Dealey RA and Whitton VJ 1998 Radiotherapy treatment planning of brain tumours using MRI alone *Br J Radiol*. **71**(845):544-8

Bourland J D and Chaney E L 1992 A finite size pencil beam model for photon dose calculations in three dimensions *Med. Phys*. **19** 1401-12.

Boyer A and Mok E 1985 A photon dose distribution model employing convolution calculations *Med. Phys*. **12** 169-77.

Chen L, Li J, Mah D, Ma CM, Wang L, Ding M, Freedman G, Movsas B and Pollack A 2002 Monte Carlo investigation of dosimetry accuracy for MR-based treatment planning. *Med. Phys*. **29**(6) 1339 (abstract)

Chen L, Price RA Jr., Li J et al 2003 Evaluation of MRI-based treatment planning for prostate cancer using a commercial TPS *Med. Phys*. Vol. **30**, no. 6, P1507

Chen L, Price R, Nguyen T-B, Wang L, J S Li, Qin L, Ding M, Palacio E, Ma C-M and Pollack A 2004 Dosimetric evaluation of MRI-based treatment planning for prostate cancer *Phys. Med. Biol*. **49** 5157-5170

Chen L, Zhu J, Xu X, Wang L, Paskalev K, Chen Z, Movsas B, and Ma C 2005 Image Guided Radiation Therapy: Investigation of Interfraction Setup and External Contour Variation for Prostate IMRT Using CT and MRI *Phys. Med* .Vol. **32** 1928

Chen Z, Ma C-M et al 2004b Investigation of CT-MR Image Intensity Correlation for MRI-based Dose calculation. *Med. Phys*., Vol.**31** No. 6 (abstract)

Debois M, Oyen R, Maes F, Verswijvel G, Gatti G, Bosmans H, Feron M, Bellon E, Kutcher G, Van Poppel H, Vanuytsel L (1999) The contribution of magnetic resonance imaging to the three-dimensional treatment planning of localized prostate cancer *Int J Radiat Oncol Biol Phys* **45** 857-65

Fransson A, Andreo P, Potter R 2001 Aspects of MR image distortions in radiotherapy treatment planning. *Strahlenther Onkol* **177**: 59-73

Guo WY 1998 Application of MR in Stereotactic Radiosurgery J. *Magn. Res. Imag*., **8**, 415-420

Jiang S B, Boyer A L, and Ma C-M 2001 Modeling the extrafocal radiation and monitor chamber backscatter for photon beam dose calculation *Med. Phys*. **28**, 55-66

Jiang S B, Deng J, Li J S, Pawlicki T, Boyer A L, and Ma C-M 2000 Modeling and commissioning of clinical photon beams for Monte Carlo treatment planning *XIII ICCR 2000* ed W Schlegel and T Bortfeld pp 434-6

Khoo VS, Adams EJ, Saran F, Bedford JL, Perks JR, Warrington AP, Brada M (2000). A comparison of clinical target volumes determined by CT and MRI for the radiotherapy planning of base of skull meningiomas *Int J Radiat Oncol Biol PhysMar* **46**1309-17

Krempien RC, Schubert K, Zierhut D, Steckner M C, Treiber M, Harms W, Mende U, Latz D, Wannenmacher M and Wenz F 2002 Open low-field magnetic resonance imaging in radiation therapy treatment planning *Int. J. Radiat. Oncol. Biol. Phys.* **53** 1350-60

Lee YK and Bollet M, 2003 Radiation Treatment Planning of Prostate Cancer Using Magnetic Resonance Imaging Alone, *Radiotherapy and Oncology* **66**:203-216

Li J S, Pawlicki T, Deng J, Jiang S B and Ma C-M 2000 Validation of a Monte Carlo dose calculation tool for radiotherapy treatment planning *Phys. Med. Biol.* **45** 2969-85

Ma C-M, Li J S, Pawlicki T, Jiang S B, Deng J, Lee M C, Koumrian T, Luxton M and Brain S 2002b A Monte Carlo dose calculation tool for radiotherapy treatment planning *Phys. Med. Biol.* **47** 1671-89

Ma C-M, Mok E, Kapur A, Pawlicki T, Findley D, Brain D S, Forster K, and A. L. Boyer A L 1999 Clinical implementation of a Monte Carlo treatment planning system *Med. Phys.* **26** 2133-43

Ma C-M, Pawlicki T, Jiang S B, Li J S, Deng J, Mok E, Kapur A, Xing Lei, Ma L and Boyer A L 2000 Monte Carlo verification of IMRT dose distributions from a commercial treatment planning optimization system *Phys. Med. Biol.* **45** 2483-95.

Mackie T R, Scrimger J W, and Battista JJ 1985 A Convolution method of calculating dose for 15-MV x rays *Med. Phys.* **12** 188-96

Mah D, Michael Hanlon SA, Freedman G, Milestone B, Mitra R, Shukla H, Movsas B, Horwitz E, Vaisanen PP and Hanks GE 2002 MRI Simulation: Effect of gradient distortions on three-dimensional prostate cancer plans Int. *J. Radiat. Oncol. Biol. Phys* **53**:757-765

Michiels J, Bosmans H, Pelgrims P, Vandermeulen D, Gybels J, Marchal G and Suetens P 1994 On the problem of geometric distortion in magnetic resonance images for stereotactic neurosurgery. *Magnetic Resonance Imaging*, **12**(5)

Mohan R 1997, Why Monte Carlo? *Proc. 12th Int. Conf. on the Use of Computers in Radiation Therapy (Salt Lake City, UT)* pp 16-8.

Oldham M and Webb S 1997 Intensity-modulated radiation therapy by means of static tomography: a planning and verification study *Med. Phys*. **24** 743-50.

Ostapiak O Z, Zhu Y, and Van Dyck J 1997 Refinements of the finite-size pencil beam model of three-dimensional photon dose calculation *Med. Phys*. **24** 743-50.

Potter R, Heil B, Schneider L, Lenzen H, Al-Dandashi C and Schnepper E (1992). Sagittal and Coronal planes from MRI for treatment planning in tumors of brain, head and neck: MRI assisted simulation *Radiother. Oncol*. **23** 127-30.

Rogers D W, Faddegon B A, Ding G X, Ma C M, We J, and Mackie R T 1995 BEAM: A Monte Carlo code to simulate radiotherapy treatment units *Med. Phys*. **22**, 503-24

Tanner S F, Finnigan D J, Khoo V S, Mayles P,Dearnalay D P and Leach M O 2000 Radiotherapy planning of the pelvis using distortion corrected MR imaged: the removal of system distortions. *Phys. Med. Biol*, **45** 2117-32.

Verhaegen F and Seuntjens J 2003 Monte Carlo modeling of external radiotherapy photon beam *Phys. Med. Biol*. **48**, R107-164

Wang X, Spirou S, Losasso T, Stein J, Chui C-S and Mohan R 1996 Dosimetric verification of intensity modulated fields *Med. Phys*. **23** 317-28.

Woo M K and Cunningham J R 1998 Comments on unified electron/photon dosimetry approach (letter) *Phys. Med. Biol*. **33** 981-2.

Yang J, Li J S, Qin L, Xiong W and Ma C-M 2004 Modeling of electron contamination in clinical photon beams for Monte Carlo dose calculation *Phys. Med. Biol*. **49** 2657-73

Yang J, Li J S, Chen L, Price R, McNeeley S, Qin L, Wang L, W Xiong and Ma C-M 2005 Dosimetric verification of IMRT treatment planning using Monte Carlo simulations for prostate cancer *Phys. Med. Biol.* **50** 1-10.

Table 1 Target dose differences between CT-based (water) and MR-based treatment plans.

Patient	ΔD_{mean}(%)	ΔD_{min}(%)	ΔD_{max}(%)	ΔD_5(%)	ΔD_{95}(%)
1	0.1	1.5	1.2	1.0	0.4
2	2.1	2.7	1.7	2.3	0.5
3	1.6	0.4	2.5	2.6	0.8
4	0.8	3.1	0.9	0.4	2.1
5	1.0	0.2	1.6	1.4	0.5
6	1.7	0.2	2.9	2.7	0.7
7	0.3	0.8	0.2	0.2	1.2
8	1.2	1.2	1.9	1.5	0.6
9	0.5	0.7	0.5	0.5	0.5
10	0.1	0.1	0.2	0.1	0.2
Average :	0.9	1.1	1.4	1.3	1.0

Table 2. Differences in target doses calculated based on MR with water equivalent uniform geometry and CT with heterogeneity correction for 10 IMRT plans of prostate cancer patients.

Patient	ΔD_{mean}(%)	ΔD_{min}(%)	ΔD_{max}(%)	ΔD_5(%)	ΔD_{95}(%)
1	1.3	1.6	1.0	1.3	1.7
2	0.5	0.5	2.1	1.0	0.5
3	1.5	1.4	0.6	0.8	1.6
4	0.9	0.3	0.3	1.2	0.9
5	1.5	1.4	1.0	1.7	1.6
6	2.6	3.2	1.7	2.7	2.7
7	2.7	1.7	3.5	3.2	1.9
8	1.3	1.2	0.7	0.9	1.4
9	2.3	2.6	2.0	2.1	2.5
10	1.5	1.9	1.3	1.1	1.4
Average :	1.6	1.6	1.4	1.6	1.6

Table 3 Differences in the target dose with and without heterogeneity correction for a 7-field, non-coplanar IMRT plan.

Beam	Gantry	Couch	Average Target dose cGy	Average Target dose (w) cGy	Δ%
1	0	0	45.4	47.0	3.40
2	275	0	20.5	22.4	8.48
3	275	340	19.8	22.2	10.81
4	280	25	38.2	40.9	6.60
5	85	20	21.6	24	10.00
6	85	0	20.7	23.1	10.39
7	85	330	38	41.4	8.21
Sum			204.2	221.0	8.27

Table 4. Differences in the target dose between MR-based calculations with different bulk densities assigned to the femurs and CT-based calculations with heterogeneity correction for a 7 beam (patient 1) and a 9 beam (patient 2) non-coplanar IMRT plan.

Patient	Density	ΔD_{mean}(%)	ΔD_{min}(%)	ΔD_{max}(%)	ΔD_5(%)	ΔD_{95}(%)
1	CT-water	7.8	6.8	9.3	8.7	6.8
	1.5	2.8	1.3	9.0	4.6	1.8
	1.8	0.1	0.8	0.4	0.8	0.9
	2.0	1.3	5.0	2.1	1.1	4.2
	2.2	3.0	7.7	1.2	0.2	6.7
2	CT-water	3.7	1.0	2.1	2.7	5.2
	1.5	1.4	1.0	1.7	1.5	1.0
	1.8	0.1	1.1	0.4	0.1	1.0
	2.0	1.0	1.6	0.4	1.0	1.0
	2.2	1.7	2.7	1.1	2.6	1.6

Table 5 Differences in the target dose after a 1.8g/cm^3 bulk-density assigned to the femurs and femoral heads for the same 7-field IMRT plan in table 3.

Beam	Gantry	Couch	Average Target dose cGy	Target dose (1.8 g/cm^3)	Δ%
1	0	0	45.4	46.2	1.7
2	275	0	20.5	19.7	4.1
3	275	340	19.8	19.9	0.5
4	280	25	38.2	38.0	0.5
5	85	20	21.6	21.9	1.4
6	85	0	20.7	20.0	3.5
7	85	330	38	38.8	2.1
Sum			204.2	204.5	2.0

Table 6 Target dose differences between CT-based (with inhomogeneity correction) and MR-based calculations (with and without bulk-density assignment) for a single beam of 6 MV and 18 MV with a 10 by 10 cm field size, gantry/couch angles at 270/340 degrees.

Patient	18 MV					6 MV				
	CT	MR(w)	%	MR(1.8)	%	CT	MR(w)	%	MR(1.8)	%
1	36.3	38.4	5.5%	34.7	4.6%	13.6	14.8	8.1%	13.0	4.1%
2	36.1	37.1	2.7%	36.7	1.6%	13.7	14.2	3.5%	14.0	2.1%
3	35.1	36.5	3.8%	35.8	2.0%	13.0	13.7	5.1%	13.3	2.3%
4	38.6	39.7	2.8%	37.8	2.1%	15.0	15.6	3.8%	14.6	2.7%
5	37.3	38.5	3.1%	37.7	1.1%	14.4	15.2	5.3%	14.7	2.0%

Figure Captions

Figure 1. Comparison of the DVHs for a co-planar plan calculated based on CT data with and without heterogeneity correction and based on MR data in uniform geometry (1 g/cm^3).

Figure 2. Isodose comparison between CT-based dose calculation without heterogeneity correction and MR-based dose calculation in uniform geometry (1 g/cm^3).

Figure 3. Comparison of DVHs for a non-coplanar plan between CT-based dose calculation with heterogeneity correction and MR-based dose calculation using homogeneous geometry.

Figure 4. Comparison of DVHs for non-coplanar plans between CT-based dose calculation with heterogeneity correction and MR-based dose calculation. Different bulk densities were assigned to the femurs in MR-based dose calculations. a) a 7 beam plan with table angles at 25^0, 20^0, 0^0, 0^0, 0^0, 340^0, and 330^0; and b) a 9 beam plan with table angle at 25^0, 20^0, 0^0, 0^0, 0^0, 0^0, 0^0, 340^0 and 335^0.

Figure 5. Comparison of the isodose distributions for a beam passing through femurs and femoral heads. A) CT with and without heterogeneity correction; B) CT with heterogeneity correction and CT water equivalent geometry with a 1.8 g/cm^3 bulk density assigned to the femurs and femoral heads.
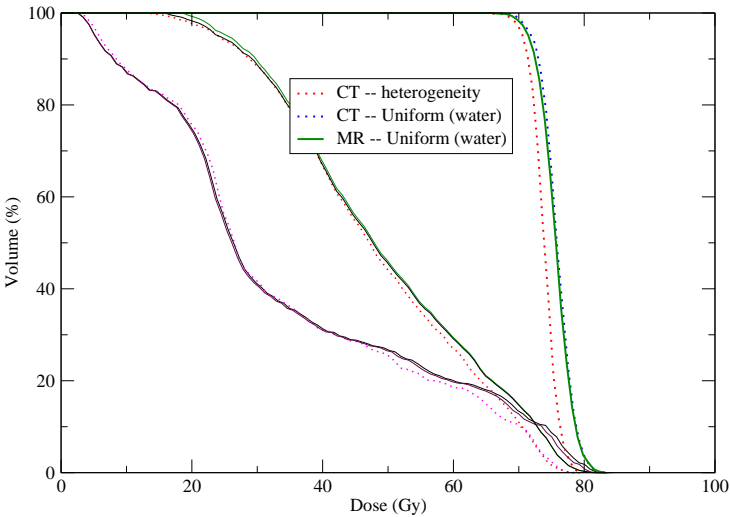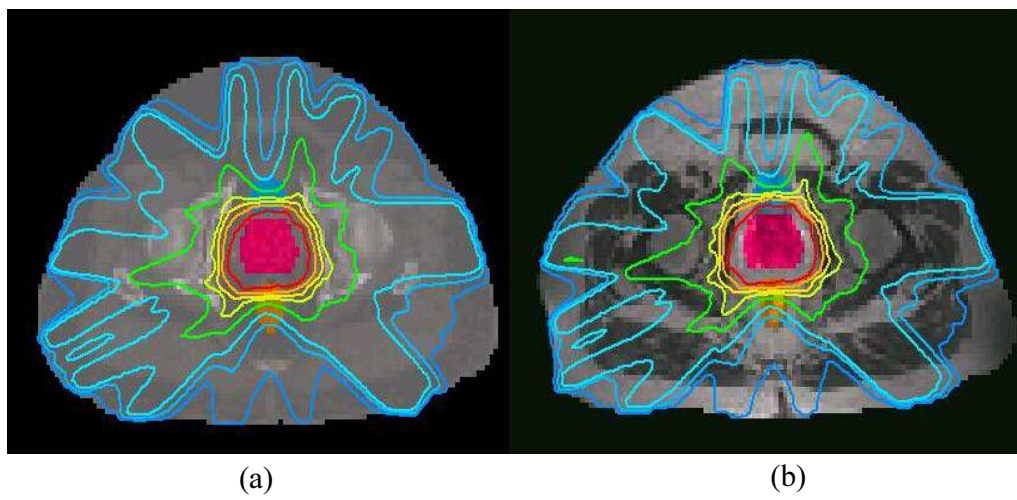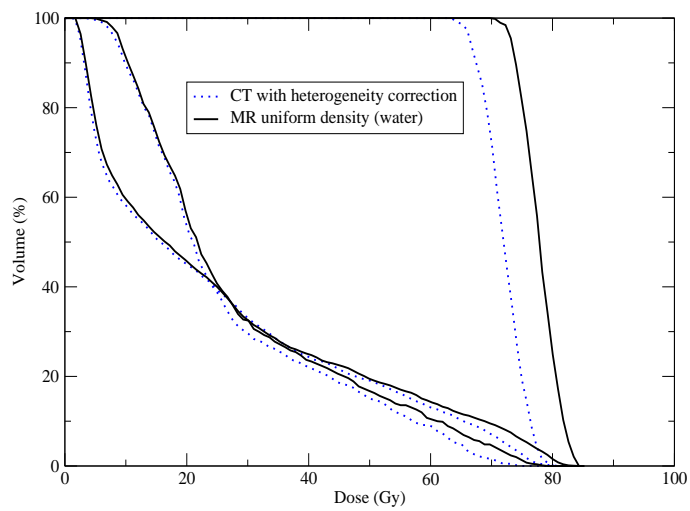
Figure 1

Figure 2

(a)   (b)
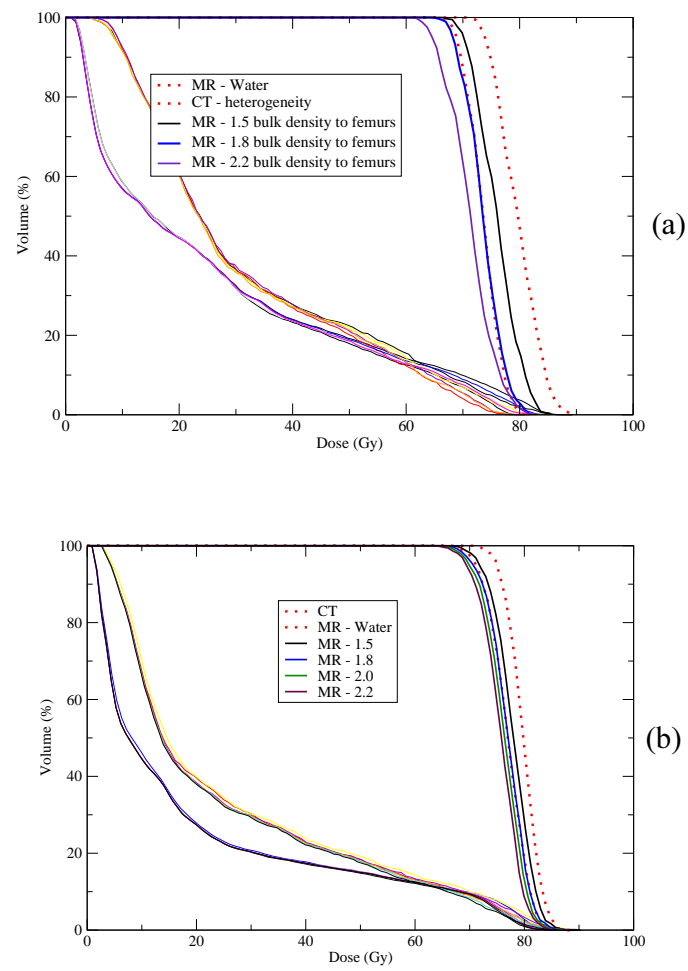
Figure 3

Figure 4

(a)

(b)

Z. Chen, et al., Monte Carlo dose verification of MRI -based treatment planning

Figure 5

(a)

(b)